Top Catal (2017) 60:152–161
DOI 10.1007/s11244-016-0726-4

ORIGINAL PAPER

Effect of Alumina Phase Transformation on Stability of Low-Loaded Pd-Rh Catalysts for CO Oxidation

Aleksey A. Vedyagin[1,2] · Alexander M. Volodin[1] · Vladimir O. Stoyanovskii[1] · Roman M. Kenzhin[1] · Pavel E. Plyusnin[3,4] · Yury V. Shubin[3,4] · Ilya V. Mishakov[1,2,4]

Published online: 26 September 2016

Abstract Bimetallic Pd-Rh catalysts with precious metal loading of 0.2 wt% was prepared by incipient wetness impregnation of the support (γ-Al_2O_3 or δ-Al_2O_3) with dual complex salt $[Pd(NH_3)_4]_3$ $[Rh(NO_2)_6]_2$. Monometallic Pd and Rh catalysts as well as its mechanical mixture were used as the reference samples. All samples were exposed for in situ prompt thermal aging procedure, and characterized by EPR spectroscopy, UV–Vis diffuse reflectance spectroscopy and photoluminescence spectroscopy. The nature of the support was found to have strong effect on high temperature stability of the samples. δ-Al_2O_3 having non-uniform phase structure due to presence of θ-Al_2O_3 and α-Al_2O_3 traces causes the concentrating of rhodium near the interphase boundary, thus changing the mechanism of Rh^{3+} bulk diffusion if compare with γ-Al_2O_3. No noticeable anchoring effects were observed for bimetallic Pd-Rh samples neither in terms of Rh bulk diffusion nor with regard to the Pd sintering. It has been found experimentally that phase transformation of γ-Al_2O_3 at high temperatures does not play dramatic role for the deactivation of bimetallic Pd-Rh active species anchored to the electron-donor site of the support.

✉ Aleksey A. Vedyagin
vedyagin@catalysis.ru

[1] Boreskov Institute of Catalysis SB RAS, Novosibirsk 630090, Russia

[2] National Research Tomsk Polytechnic University, Tomsk 634050, Russia

[3] Nikolaev Institute of Inorganic Chemistry SB RAS, Novosibirsk 630090, Russia

[4] Novosibirsk State University, Novosibirsk 630090, Russia

Keywords Bimetallic Pd-Rh catalysts · CO oxidation · Alumina · Thermal aging · Deactivation · Stability · Phase transformation

1 Introduction

Since the discovery of internal-combustion engine and beginning of automobile era till present days the problem of effective neutralization of exhaust gases remains the most actual in the field of environmental science. In order to solve this problem in respect to the more widespread gasoline engines the catalysts containing Pt, Pd and/or Rh supported on oxide carriers (Al_2O_3, CeO_2, ZrO_2 etc.) can be applied [1]. In the last decades the researchers avoid using platinum and tend to prefer the Pd-only systems or bimetallic Pd/Rh compositions [2, 3]. As a rule, gamma or gamma/delta/theta alumina are used as a support for the main active component [4–8]. From other hand, in order to increase the thermal stability of the support as well as to enhance the oxygen storage capacity (OSC function) the alumina is often doped with zirconia and/or oxides of rare-earth elements (Ce, La, Y etc.) [9–13].

A problem of stability of the precious metals (PM) containing catalysts is of special importance. It is known that a relatively small loading of the PM allows reaching the acceptable activity in such reactions as CO and hydrocarbons oxidation and nitrogen oxides reduction. However, in the course of operating, especially in the long run, a major part of the active component is deactivated, and the remaining amount of active Pd and/or Rh is not enough to provide the required level of the activity of the catalytic composition in general. The literature lists the following processes taking place at elevated temperatures as the main reasons for deactivation: sintering of palladium

and formation of large agglomerates; interaction of rhodium with OH-groups of the support, transition into ionic form and diffusion of ions into the support volume; surface diffusion of Pd and Rh resulting in the formation of thermodynamically stable alloyed particles [14–17]. It was shown in our previous works [18, 19] that the formed Rh ions diffuse into the support bulk and cause the phase transformation of γ-alumina into α-phase already at a temperature of 1000 °C.

To solve the problem of Pd/Rh catalysts deactivation we have used two approaches in our studies: securing the active components as clusters on the electron-donor sites of the support (γ-Al_2O_3) [20] and forming bimetallic Pd-Rh particles, which hinders the transition of Rh into ionic form followed by its diffusion into the bulk [19, 21]. As was mentioned above, the formation of Pd-Rh alloy is one of the reasons for deactivation of these catalysts, however, the catalyst operation conditions form the thermodynamically stable alloys [22]. On the other hand, it is known that Pd/Rh system features a limited region of existence of solid solutions [23]. The immiscibility region present on the phase diagram gives grounds to talk about the possibility of the synthesis of thermodynamically metastable Pd-Rh alloys with rhodium content $17\ \% < X_{Rh} < 83\ \%$. We have shown [19, 21] that the catalysts based on these alloys are as good as the monometallic samples and their mechanic mixtures in activity, and are significantly better in stability.

One of the parameters showing the thermal stability of the catalysts is the ability to keep the catalytic activity at an acceptable level after the procedure of thermal aging. The temperature of the procedure can differ depending on the conditions of aging and the studied factors, however, it usually lies within the range $800 \leq T_{ag} \leq 1300$ °C. The behavior of catalytic systems at a temperature up to 1000–1050 °C is being particularly interesting [23–27]. We should note that at the high temperatures the phase changes of γ-oxide to δ (above 800 °C) and further to θ (above 1000 °C) are expected [28]. An impact of the alumina nature (phase modification) over the deactivation of Pd-Rh catalysts is barely ever discussed in literature. The given work is dedicated to the study of this influence as well as of the role of the support phase changes in these processes.

2 Experimental

2.1 Preparation of the Catalysts

γ-Al_2O_3 and δ-Al_2O_3 supports used in this research were prepared by calcination of commercial $Al(OH)_3$ hydroxide (Condea) for 6 h at 720 and 1000 °C, respectively. Prior the calcination the oven was heated up starting from room temperature with ramping rate of 1.5 °C/min. Incipient wetness impregnation of the support with dual complex salt $[Pd(NH_3)_4]_3$ $[Rh(NO_2)_6]_2$ was used to prepare alloyed Pd-Rh catalysts. The concentrations of the complexes were selected to obtain the total metal concentration 0.2 wt%. The impregnated samples were dried in a furnace at 105 °C for 4 h, then heated in air at 400 °C at the heating rate 10 °C/min, and allowed to stay for 1 h at this temperature. The calcined samples were triply boiled in distilled water, filtered out of $NaNO_3$ using a porous filter and dried in a furnace at 105 °C for 4 h. The atomic Pd/Rh ratio in the prepared samples was 3/2.

Reference samples were synthesized by separate incipient wetness impregnation of identical weighted alumina samples with solutions of complexes $[Pd(NH_3)_4](NO_3)_2$ and $Na_3[Rh(NO_2)_6]$. The concentrations of the complexes were 0.24 and 0.16 wt%, respectively, to maintain the identical ratio and concentrations of the metals in the mechanical mixture and in the bimetallic catalyst. The samples were dried and calcined using the procedures described above. Then, they were thoroughly ground in an agate mortar for homogenization. Monometallic samples containing 0.12 wt% Pd and 0.08 wt% Rh were synthesized using the same procedure. The description of the prepared samples is presented in Table 1.

2.2 Characterization Procedures

Specific surface area (S_{BET}), pore volumes and average pore diameters of the supports were determined by low-temperature nitrogen adsorption/desorption using an ASAP 2400 instrument.

The phase composition of the supports was studied in 2θ range 15–75° (0.05° step size) on a Shimadzu XRD-7000 diffractometer (CuKα radiation, Ni filter on the reflected beam, and a scintillation detector with amplitude discrimination). Interpretation of the diffraction patterns was done

Table 1 Description of the prepared samples

#	Sample	Pd, wt%	Rh, wt%	Type	Support
1	PdRh(g)bim	0.12	0.08	Bimetallic	γ-Al_2O_3
2	PdRh(g)mix	0.12	0.08	Mixture	γ-Al_2O_3
3	Pd(g)mono	0.12	–	Mono	γ-Al_2O_3
4	Rh(g)mono	–	0.08	Mono	γ-Al_2O_3
5	PdRh(d)bim	0.12	0.08	Bimetallic	δ-Al_2O_3
6	PdRh(d)mix	0.12	0.08	Mixture	δ-Al_2O_3
7	Pd(d)mono	0.12	–	Mono	δ-Al_2O_3
8	Rh(d)mono	–	0.08	Mono	δ-Al_2O_3

using data for pure compounds reported in the JCPDS-ICDD database [29].

Electron paramagnetic resonance (EPR) spectroscopy was performed using an ERS-221 EPR spectrometer operating in the X-band ($\nu = 9.3$ GHz). EPR spectra were acquired at 20 dB attenuation with typical microwave power 3 mW. The frequency of the microwave irradiation and the magnetic field were measured using a ChZ-64 frequency meter and a Radiopan MJ-100 magnetometer, respectively. EPR-CAD software package was used to control the spectrometer operation and analyze the results obtained. Radical anions of aromatic nitro compounds arising from their adsorption on the surface of oxide catalysts were used as spin probes for the study of surface electron-donor sites [19, 20, 30]. A catalyst sample ($\sim$20 mg) was loaded in a quartz ampoule, heated at 170 °C for 12 h, and then cooled down to room temperature. 2×10^{-2} M 1,3,5-trinitrobenzene (TNB) solution in toluene was added to launch the formation of the anion radicals. The temperature was then maintained at 80 °C for 12 h for further acceleration of the radical anion formation to their maximum, which corresponds to the concentration of surface electron-donor sites. The EPR spectra of generated radical anions were recorded at room temperature. The concentrations of the paramagnetic species were determined by numerical double integration with baseline compensation.

Photoluminescence (PL) experiments were carried out under atmospheric conditions at 290 K using a Cary Eclipse (Varian) spectrofluorimeter. A 532-nm frequency-doubled Nd:YAG DPSS laser was used for the luminescence excitation. A powder sample was placed in a short light path (0.8 mm) UV quartz cell in a front-face configuration.

UV–Vis diffuse reflectance spectra were recorded between 200 and 800 nm using a UV–Vis spectrometer UV–Vis 2501 PC (Shimadzu) with IRS-250A diffusion reflection attachment. The UV–vis spectra were transformed into the Kubelka–Munk function F(R) calculated as $F(R) = (1 - R)^2/2R$, where R is the experimentally measured reflectivity coefficient of the samples [31].

2.3 Thermal Aging and Prompt Thermal Aging Procedures

The thermal stability of the samples was studied using the in situ prompt thermal aging procedure (PTA) [19]. CO conversion was used as a chemical response to follow the catalytic behavior and state of active components during the procedure. The sample (300 mg) was loaded into quartz flow reactor, and then reaction mixture contained 0.15 vol. % CO, 14.0 vol. % O_2 and N_2 as balance was passed through the reactor. The flow rate was 334 ml/min. Temperature ramping rate was 10 °C/min. The samples underwent two light-off cycles at 50–320 °C, two cycles at 50-600 °C, and finally three cycles at 50-800 °C. Changes in the CO concentration in the outlet flow were registered by a gas analyzer ULTRAMAT 6 (Siemens). The temperature of 50 % CO conversion was used as the criterion to compare the catalyst activity and stability.

Additionally, all samples were subjected to high temperature thermal aging procedure (PTA-1 k). Each sample was placed into quartz flow reactor and heated up to 1000 °C with ramping rate of 10 °C/min in the same reaction flow. The duration of high temperature step was 6 h. Some samples were calcined in muffle furnace at 700 °C after PTA-1 k procedure (labeled as PTA-1 k-700).

3 Results and Discussion

It is well known that alumina exists as several metastable crystal structures and thermodynamically stable α-phase [28, 32, 33]. As a result of the temperature impact the support undergoes the structural phase transformations (from tetragonal γ and δ to monoclinal θ and hexagonal α), specific surface decreases, and the surface properties change. The nucleation-growth mechanism is realized along the way, and the size of crystallites grows from 20 nm for γ to 70–150 nm for α [34]. Since this process happens in stages, at a certain moment of time the support stops being homogeneous in its phase composition, the nuclei of the new phases form, and as a result the areas of local straining appear. Figure 1 presents the XRD data for the support samples treated at different temperatures. The X-ray patterns confirm the presence of solely γ-Al_2O_3-phase in the case of sample calcined at 720 °C. Treatment

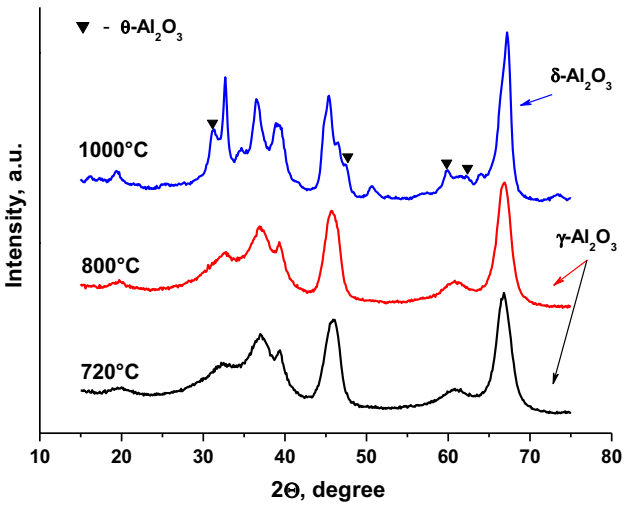

Fig. 1 XRD patterns of the alumina samples calcined at different temperatures

at 800 °C gives γ-Al_2O_3 with the trace amounts of δ-phase. Calcination of the support at 1000 °C results in a transition into δ-Al_2O_3-phase, with an insignificant admixture of α-Al_2O_3 and θ-Al_2O_3 phases (<1 %). It should be noted that the presence of the small admixture of these phases in this sample is reliably detected by the luminescent methods. According to the PL spectra of impurity Cr^{3+} ions the initial δ-Al_2O_3 support contained less than 0.01 % of α-Al_2O_3 and about 0.1–0.2 % of θ-Al_2O_3. The relative calibration of the PL method in determination of the α-Al_2O_3 concentration was provide using the starting alumina calcined in air at 1200 °C (12 h) as a Ref. [18]. It is also known that θ-phase differs from γ and δ in density (3.2 g/cm^3 for γ and δ, 3.56 g/cm^3 for θ) [28]. Therefore, we can suppose that δ-Al_2O_3 support used in the present work is characterized by a structure with local non-uniformities and distortions.

Table 2 gives the values of the specific surface, pore volume and average pore diameter for these three support samples. It is evident that the treatment of the support at 800 °C results in an insignificant change in the pore volume, whereas the values of the average diameter and specific surface decrease for 7 %. After the calcination at 1000 °C the pore volume drops for 20 %, average diameter, for 33 %, and specific surface, for 39 %. Therefore, we can conclude here that the study of influence of the support nature on the catalysts state need to be performed at temperatures up to 800 °C, when γ-Al_2O_3 and δ-Al_2O_3 are not subjected to significant changes, both in phase and texture. Characterization of the catalyst samples processed at the temperatures above 800 °C should help to evaluate the distribution of the phase changes into their deactivation.

To study the thermal stability of the catalysts depending on the support nature the procedure of prompt thermal aging (PTA) was used. The method is based on the gradual elevation of the maximum temperature of the cycle at cyclic heating–cooling of the catalyst in the reaction flow. As an example, Fig. 2 shows the light-off curves in PTA cycles for the PdRh(d)bim sample. The first cycle reflects the interaction of the reaction mixture with the fresh sample. At a temperature above 250 °C the state of the active sites stabilizes (a possible reduction of the surface oxides of metals), and weakly bound hydroxyl groups are removed, resulting in a significant decrease in the activity in the second cycle. The comparison of the curves of the second and third cycles characterizes the stability of the system at 320 °C, fourth and fifth, at 600 °C, and sixth and seventh, at 800 °C.

Table 2 Textural properties of alumina calcined at different temperatures

Temperature, °C	BET surface area, m^2/g	Pore volume, cm^3/g	Average pore diameter, Å
720	182.5	0.538	117.9
800	168.5	0.533	126.4
1000	110.7	0.435	157.3

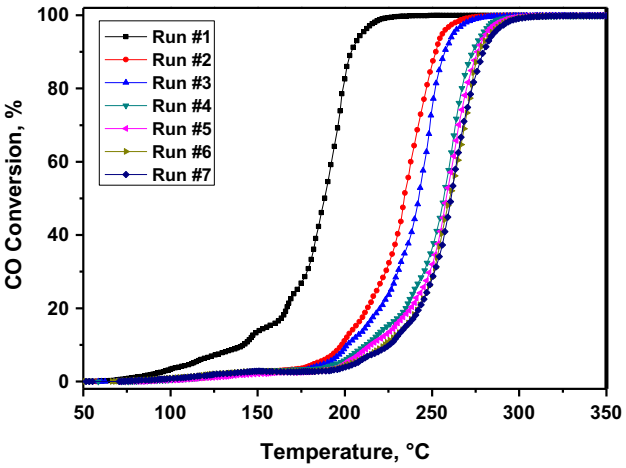

Fig. 2 Light-off curves for bimetallic PdRh(d)bim sample

Figure 3 represents the temperatures of 50 % conversion of CO (T_{50}) depending on the PTA cycle number. For the monometallic Rh samples the data are given beginning with the third cycle, since at the temperatures below 350 °C the CO conversion never reached 50 %. As shown in Fig. 3a, in case of the monometallic Pd samples the support nature does not play a significant role, whereas for the bimetallic Pd-Rh catalysts δ-Al_2O_3 is a preferable support. The PdRh(d)bim sample exceeds the compared samples both in the initial activity and stability. The same conclusion follows from Fig. 3b for the monometallic Rh sample Rh(d)mono.

Previously we have shown that the spin-probed electron-donor sites of the γ-Al_2O_3 surface are important for stabilizing the supported palladium in the form of atomic-dispersed ions Pd^{2+}. It is these states of the supported palladium that show high activity in the reaction of CO oxidation [20]. Further studies have shown that the spin probes are also a useful tool for studying the properties of the active sites of binary Pd-Rh catalysts [19, 21]. For all catalysts studied in these works we used γ-Al_2O_3. As has been noted, in the thermal aging this oxide is subjected to the phase changes at a temperature above 900 °C, and at 1000 °C it turns to δ-phase almost completely. This phase has a noticeably smaller specific surface area (Table 2), and its formation is inevitable for the catalysts working at high temperatures. At the same time δ-Al_2O_3, like γ-phase, has the electron-donor sites, the concentration of which with regard to the surface unit is close to those on γ-phase [35].

An important feature of δ-phase is its stability at the temperatures of thermal aging. It means that the processes of

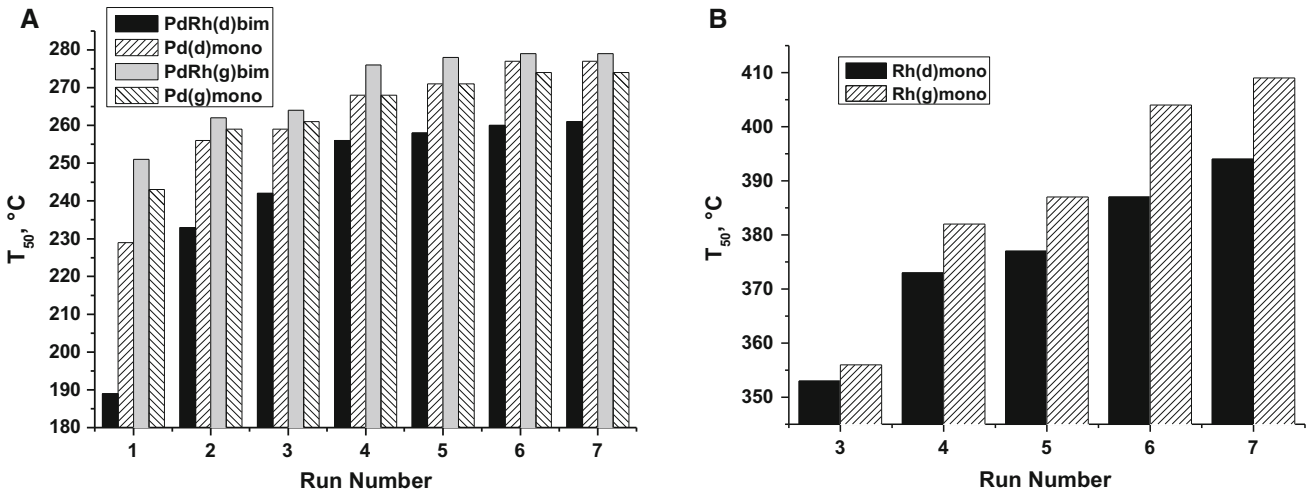

Fig. 3 T_{50} vs. run number for: **a** monometallic Pd and bimetallic Pd-Rh samples; **b** monometallic Rh samples

evolution of the active sites of the catalysts supported on this phase are immune to the effects related to the structure changes of the support as a result of its phase transformations.

Figure 4 demonstrates the typical EPR spectra of spin probes, the concentration of which reflects the concentration of the active sites of Pd-containing catalysts. The obtained results bear evidence that the concentration of such sites for the initial catalysts with δ- and γ-alumina used as supports is close and reflects the amount of the supported Pd (Fig. 4a, c). For the Rh-only catalyst the concentration of spin probes is minimal and corresponds to that of the support.

The result is rather natural, since with the used concentrations of the supported metals (less than 0.2 wt%) the number of the donor sites on the support surface (able to stabilize the isolated Pd^{2+} ions) significantly exceeds the number of supported Pd atoms.

Behavior of the Pd-containing active sites on the surface of δ-Al_2O_3 and γ-Al_2O_3 changes dramatically after thermal aging at 1000 °C in PTA regime (Figs. 4b, d, 5a). It is seen well that as a result of this treatment the concentration of the active sites for the PdRh(g)bim sample on γ-Al_2O_3 does not change, decreases slightly for Pd(g)mono, and drops significantly only for PdRh(g)mix (Fig. 5a); at the same time for all catalysts on δ-Al_2O_3 all samples invariably show a large decrease in the concentration of the active sites. Therefore, in spite of the absence of the phase transformations of the support for the catalysts based on δ-Al_2O_3 deactivation of Pd-containing active sites at a temperature above 800 °C on them is expressed much stronger than on γ-Al_2O_3. The reasons for this phenomenon are not clear yet and are likely to be due to facilitation of the course of surface diffusion and agglomeration of the atomic-dispersed ion species of Pd on δ-Al_2O_3 as compared with that of γ-Al_2O_3.

An important result of this study is a detection of high thermal stability of the active sites on PdRh(g)bim catalyst in PTA regime, which shows the effect of stabilization of Pd-containing active sites due to interaction with Rh. It is clearly seen that the mechanic mixture PdRh(g)mix containing a similar integral concentration of precious metals does not feature such properties. At the same time it is quite evident that the use of δ-Al_2O_3 is senseless in terms of an increase in thermal stability of the catalysts at high temperatures.

Both series of the catalysts were characterized with UV–Vis diffuse reflectance (DR) method. In all Pd-containing samples initially palladium is contained in the form of isolated forms Pd^{2+} and PdO particles of small size with the values of band gap energy E_g ~1.6–1.7 eV. Note that somewhat smaller average size of PdO particles are typical of Pd(g)mono (E_g ~1.75 eV) as compared with those of Pd(d)mono sample (E_g ~1.75 eV).

UV–Vis DR spectra for fresh samples on δ-Al_2O_3 (calcined at 600 °C) are presented in Fig. 6. All spectra excluding one for Rh(d)mono were normalized to 1 in a peak region of d–d transition band for Pd^{2+} ions.

For Pd(d)mono, PdRh(d)mix and PdRh(d)bim samples the dominating contribution is due to d–d transition band of Pd^{2+} at 450 nm and palladium-oxygen charge transfer band at 250 nm [36, 37]. Spectrum for 0.125 %Pd/Al_2O_3 sample calcined at 630 °C (along with approximation by single Gaussian function) is shown here a reference one. This reference sample prepared using H_2PdCl_4 (Merk) as Pd precursor is known to have all supported palladium in a state of isolated Pd^{2+} ions (band gap energy E_g ~1.88 eV).

The formation of PdO particles causes the appearance of band gap (E_g) which value decreases along with growth of particle size starting from ~1.9 eV for isolated Pd^{2+} ions [38] down to 0.8 eV for bulk PdO [39].

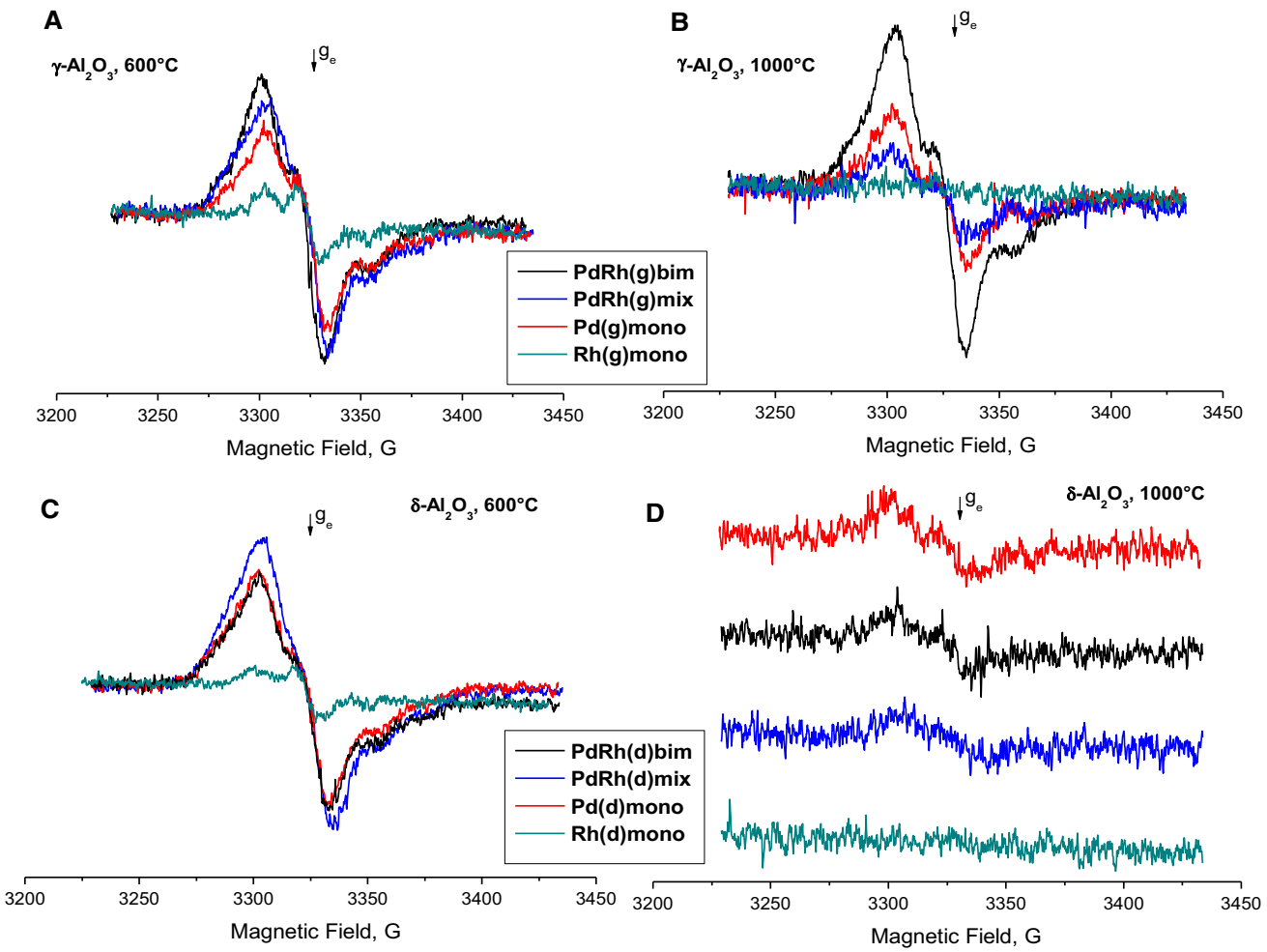

Fig. 4 EPR spectra of TNB anion radicals: **a** γ-Al_2O_3 series calcined at 600 °C; **b** γ-Al_2O_3 series after PTA-1 k; **c** δ-Al_2O_3 series calcined at 600 °C; **d** δ-Al_2O_3 series after PTA-1 k

The diffuse reflectance spectrum for Rh(d)mono (Fig. 6) correspond to surface Rh^{3+} complexes with allowed transitions $^1A_{1g} \rightarrow {}^1T_{1g}$, $^1T_{2g}$ at 440 and 340 nm accordingly and a charge transfer band with the edge at 200 nm [18]. It is noticeable that in the case of Rh(d)mono or any other Rh-containing non-alloyed samples rhodium leaves the surface during the high-temperature treatment (above 600 °C) in air or at PTA-1 k conditions. As a result the intensity of the $^1T_{1g}$ band diminishes in one order of magnitude (if compare with d–d transition of Pd^{2+}) due to decrease of the extinction coefficient caused by the decoration of Rh^{3+} ions with the support.

Figure 7 shows UV–Vis DR spectra for Pd(d)mono (1) and Pd(g)mono (2) samples after PTA-1 k. The shift of d–d absorption band for Pd^{2+} ions to 380 nm which is close to the reference value for $Pd(H_2O)_4^{2+}$ at 378 nm [40, 41] was found to be a common trait for both samples. As a rule, at the state of equilibrium on air the partial substitution of the oxygen neighborhood of Pd^{2+} with OH^- takes place resulting in formation of the structures similar to $Pd(OH)_4^{2-}$ with d–d absorption band at 405-420 nm, since OH^- is a weaker ligand than H_2O.

As it follows from Fig. 7, Pd(g)mono-PTA-1 k sample qualitatively differs from others by narrow distribution of d–d absorption band for Pd^{2+} ions at 380 nm. Spectrum for Pd(d)mono-PTA-1 k is characterized by wider distribution of band at 380 nm and structureless absorption band at 650–850 nm due to the presence of agglomerated Pd^0 metal particles [42]. The appearance of shoulder at 490–520 nm indicates the presence of relatively large PdO particles with no partial substitution of ligands at PTA-1 k conditions. It should be also noted that additional calcination of Pd(g)mono-PTA-1 k and Pd(d)mono-PTA-1 k samples in muffle furnace at 700 °C during 6 h has returned the system back to initial state with oxygen neighborhood of Pd^{2+}. The corresponding spectra for Pd(d)mono-PTA-1 k-700 and Pd(g)mono-PTA-1 k-700 are also presented in Fig. 7. No additional sintering of PdO

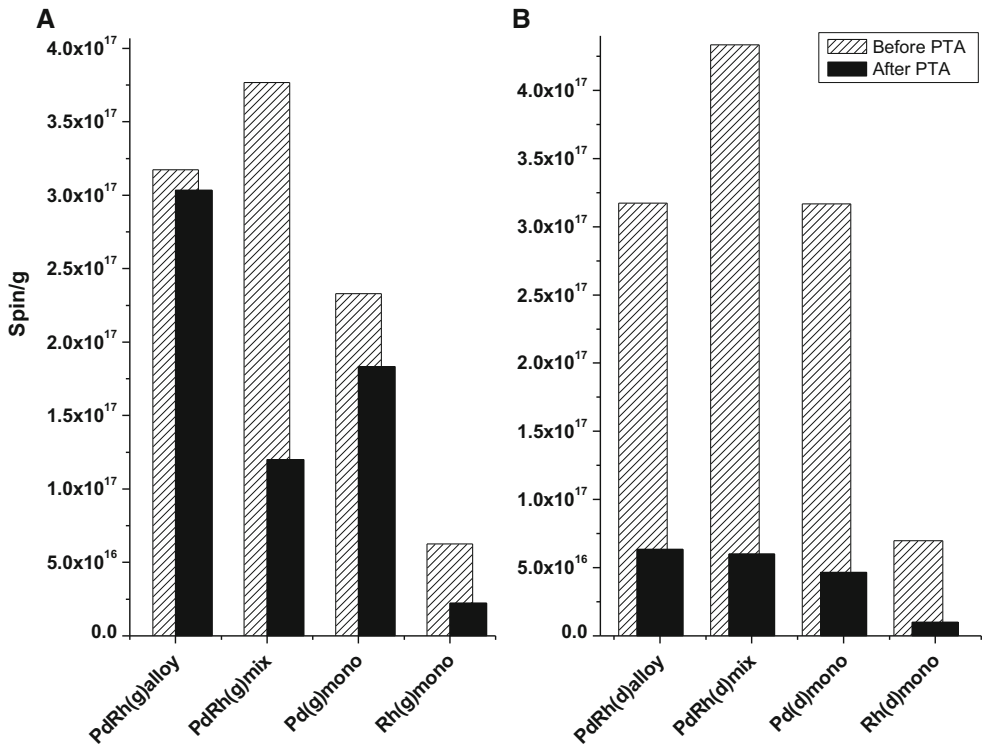

Fig. 5 Concentration of TNB anion radicals before and after PTA-1 k procedure: **a** γ-Al_2O_3 series; **b** δ-Al_2O_3 series

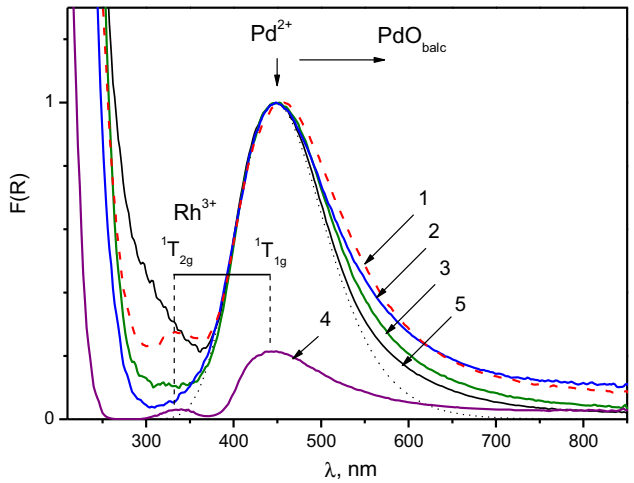

Fig. 6 UV-Vis DR spectra for fresh samples of δ-Al_2O_3 series: PdRh(d)bim (1); PdRh(d)mix (2); Pd(d)mono (3); Rh(d)mono (4). All spectra excluding one for Rh(d)mono were normalized to 1 in a peak region of d–d transition band for Pd^{2+} ions. Spectrum for 0.125 %Pd/Al_2O_3 calcined at 630 °C (5) along with its approximation by single Gaussian function (*dots*) is given for comparison

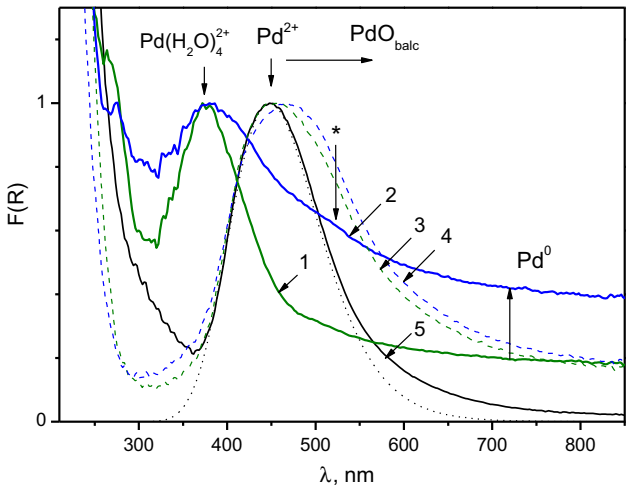

Fig. 7 UV-Vis DR spectra for Pd(g)mono (1, 3) and Pd(d)mono (2, 4) samples after PTA-1 k (1, 2) and PTA-1 k-700 (3, 4). Spectrum for 0.125 %Pd/Al_2O_3 calcined at 630 °C (5) along with its approximation by single Gaussian function (*dots*) is given for comparison

was observed to be resulted by this thermal treatment. At the same time, PdO particles are increased in size comparing with initial state (Fig. 6). From these two samples Pd(g)mono-PTA-1 k is characterized with relatively small average size of PdO particles (E_g ~1.51 eV) and larger part of isolated Pd^{2+} species in comparison with Pd(d)-mono-PTA-1 k (E_g ~1.46 eV).

Figure 8 demonstrates UV–Vis DR spectra for PdRh(g)bim (1) and PdRh(g)mix (2) samples pretreated at PTA-1 k conditions. It can be concluded here that spectrum for PdRh(g)bim-PTA-1 k is qualitatively similar to that of

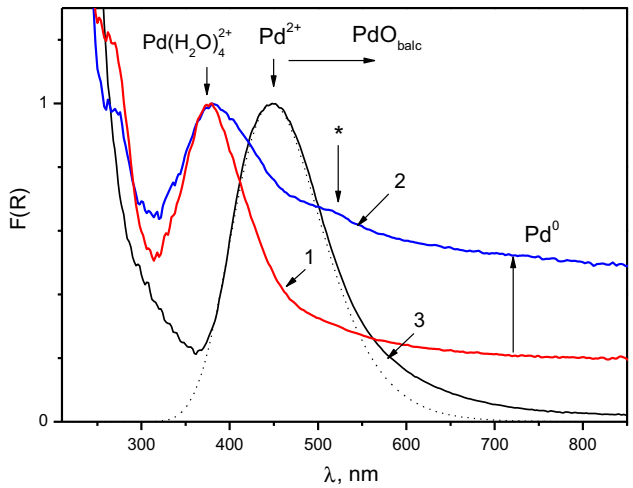

Fig. 8 UV-vis DR spectra for PdRh(g)bim-PTA-1 k (1) and PdRh(g)mix-PTA-1 k (2) samples. Spectrum for 0.125 %Pd/Al_2O_3 calcined at 630 °C (3) along with its approximation by single Gaussian function (*dots*) is given for comparison

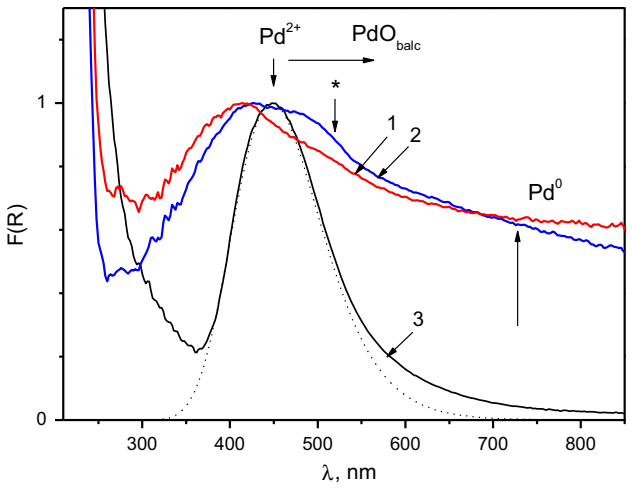

Fig. 9 UV-vis DR spectra for PdRh(d)bim-PTA-1 k (1) and PdRh(d)mix-PTA-1 k (2) samples. Spectrum for 0.125 %Pd/Al_2O_3 calcined at 630 °C (5) along with its approximation by single Gaussian function (*dots*) is given for comparison

Pd(g)mono-PTA-1 k (Fig. 7) and characterized with narrow d–d absorption band for Pd^{2+} ions at 380 nm.

As seen from the Fig. 8, spectrum for PdRh(g)mix-PTA-1 k sample also contains increased shoulder at 490–520 nm which is intrinsic to large PdO particles. Another shoulder at 405-402 nm corresponds to the part of structures similar to $Pd(OH)_4^{2-}$. Higher intensity of absorption band indicates the presence of agglomerated Pd^0 metal particles. Comparing the spectra for PdRh(g)bim and PdRh(g)mix samples allows one to conclude that in the case of bimetallic alloyed catalyst Pd and Rh species are mutually anchored, thus preventing sintering of palladium.

UV–Vis DR spectra for PdRh(d)bim and PdRh(d)mix samples subjected to PTA-1 k treatment are presented in Fig. 9. According to the position of d–d absorption band for Pd^{2+} in spectra, both samples contain structures similar to $Pd(OH)_4^{2-}$, large PdO particles and agglomerated Pd^0 particles. In this case no considerable mutual anchoring of Pd and Rh species is observed.

As we have reported recently [19], the effect of Pd-Rh mutual anchoring can also be appeared in diminution of Rh amount diffused into the bulk of support at high temperatures (above 800 °C).

In the α-Al_2O_3 structure Rh^{3+} ($4d^6$) ions occupying low-spin octahedral positions are characterized by a phosphorescence band at 650 nm [18]. This approach was used in present work to study the bulk diffusion of rhodium and to estimate it quantitatively.

Figure 10 shows photoluminescence spectra for Rh^{3+} excited at 390 nm and Cr^{3+} excited at 565 nm for PdRh(g)bim and PdRh(g)mix samples after PTA-1 k-700 procedure. The spectra were obtained at identical conditions and subject to different optical density of the samples for E_{exi} = 390 nm and E_{exi} = 565 nm as described in [20]. Both PdRh(g)bim-PTA-1 k-700 and PdRh(g)mix-PTA-1 k-700 samples are characterized with a presence of θ-Al_2O_3 and α-Al_2O_3 traces, and luminescence of Rh^{3+} in α-Al_2O_3. As follows from the spectra, Rh concentration in alumina bulk is noticeably lower in the case of PdRh(g)bim-PTA-1 k-700 sample, thus indicating the Pd-Rh anchoring effect. Contrariwise, in the case of δ-Al_2O_3 (Fig. 11) close values of luminescence intensities for Rh^{3+} ions encapsulated in the corundum phase as well as for R_α Cr^{3+} (694 nm) and R_θ Cr^{3+} (685 nm) peaks attributed to α-Al_2O_3 and θ-Al_2O_3, respectively testify towards weak Pd-Rh interaction and absence of noticeable mutual anchoring of the metals.

The most exciting result was observed for the monometallic Rh(g)mono and Rh(d)mono samples

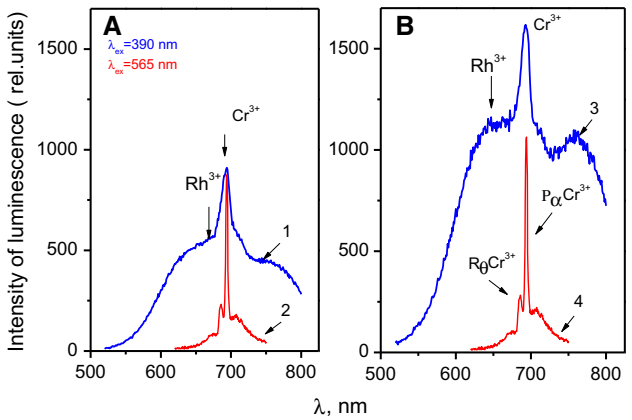

Fig. 10 Photoluminescence spectra for Rh^{3+} (1, 3) and Cr^{3+} (2, 4) for PdRh(g)bim-PTA-1 k-700 (**a**) and PdRh(g)mix-PTA-1 k-700 (**b**) samples obtained at identical conditions

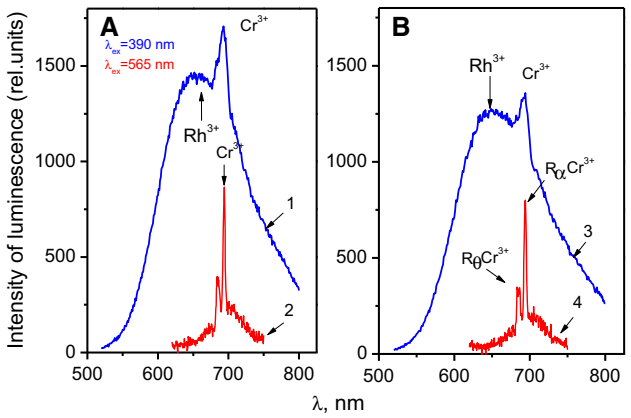

Fig. 11 Photoluminescence spectra for Rh^{3+} (1, 3) and Cr^{3+} (2, 4) for PdRh(d)bim-PTA-1 k-700 (**a**) and PdRh(d)mix-PTA-1 k-700 (**b**) samples obtained at identical conditions

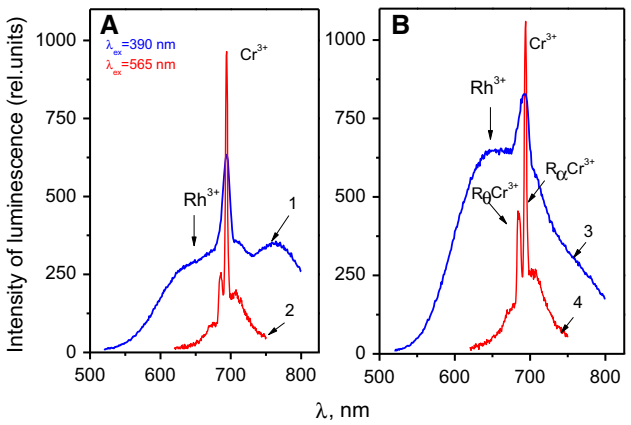

Fig. 12 Photoluminescence spectra for Rh^{3+} (1, 3) and Cr^{3+} (2, 4) for Rh(g)mono-PTA-1 k-700 (**a**) and Rh(d)mono-PTA-1 k-700 (**b**) samples obtained at identical conditions

calcined in PTA-1 k-700 conditions. As follows from Fig. 12, the amounts of α-Al_2O_3 and θ-Al_2O_3 phases determined from luminescence intensities are relatively close to each other. At the same time, the intensity of Rh^{3+} (E_{exi} = 390 nm) for Rh(d)mono-PTA-1 k-700 is in about 2 times higher. It can be supposed here that in this case the mechanism of Rh bulk diffusion has changed resulting in rhodium concentrating near the interphase boundaries of θ and δ phases of alumina. This process takes place at temperatures above 600 °C and appears in increasing of local concentration of Rh^{3+} at higher temperatures when corundum phase formation occurred.

4 Conclusions

Two series of PM-containing catalysts based on γ-Al_2O_3 and δ-Al_2O_3 were synthesized and studied in the present work. It is revealed that with the use of γ-Al_2O_3 the phase transformations of support in the high-temperature region (above 800 °C) are not crucial in terms of deactivation of bimetallic Pd-Rh catalysts. Strong interaction of active species with donor sites of support as well as mutual anchoring of metals provides good stability along with appropriate activity of the samples. The nature of support plays a far more important role. The impact of high temperature treatment on the state of systems based on γ- and δ-alumina is different despite the similar catalytic behavior and stability of fresh samples at temperatures below 800 °C. Thus, initially PdRh(d)bim sample seemed to be more active and stable in comparison with PdRh(g)bim. However, Rh was found to diffuse into bulk of δ-Al_2O_3 during the thermal aging procedure (1000 °C) in all cases including bimetallic sample. Structural and phase non-uniformity of this support causes concentrating of Rh near the interphase boundaries of δ-Al_2O_3 and θ-Al_2O_3 phases. Moreover, intensified sintering of palladium particles was found to take place on δ-alumina. Finally we can conclude that the effect of Pd-Rh mutual anchoring observed for PdRh(g)bim catalyst is not proper for the sample based on δ-Al_2O_3.

Acknowledgments This work was supported by Russian Academy of Sciences and Federal Agency of Scientific Organizations (project V.45.3.2). The authors are grateful to M.S. Mel'gunov, T.Ya. Efimenko, and T.A. Komnik for their assistance in catalyst testing and characterization.

References

1. Heck RM, Farauto RJ (2002) Catalytic air pollution control: commercial technology, 2nd edn. Wiley, New York
2. Renzas JR, Huang WY, Zhang YW, Grass ME, Hoang D, Alayoglu S, Butcher DR, Tao F, Liu Z, Somorjai GA (2011) Phys Chem Chem Phys 13:2556–2562
3. Renzas JR, Huang WY, Zhang YW, Grass ME, Somorjai GA (2011) Catal Lett 141:235–241
4. Williamson WB, Linden DG, Summers JC (1991) High-temperature three-way catalyst for treating automotive exhaust gases. U.S. Patent 5,041,407
5. Williamson WB, Silver RG, Summers JC (1997) Paladium-containing three-way automotive catalysts having unique support. U.S. Patent 5,672,557
6. Foong JS, Rabinowitz HN (2003) Hydrogen sulfide-suppressing catalyst compositions. U.S. Patent Application Publication 2003/0158037
7. Nunan JG et al. (2012) Three-way catalyst having an upstream single-layer catalyst. U.S. Patent Application Publication 2012/0128557
8. Nunan JG et al. (2012) Three-way catalyst having an upstream multi-layer catalyst. U.S. Patent 8,323,599
9. He H, Dai HX, Wong KW, Au CT (2003) Appl Catal A Gen 251:61–74
10. Wu X, Wu X, Liang Q, Fan J, Weng D, Xie Z, Wei S (2007) Solid State Sci 9:636–643
11. Fan J, Wu X, Yang L, Weng D (2007) Catal Today 126:303–312
12. He X, Sun J, Huan Y, Hu J, Yang D (2010) J Rare Earth 28:59–63

13. Zhao B, Wang Q, Li G, Zhou R (2013) J Environ Chem Eng 1:534–543
14. López Granados M, Cabello Galisteo FC, Mariscal R, Alifanti M, Gurbani A, Fierro JLG, Fernández-Ruíz R (2006) Appl Surf Sci 252:8442–8450
15. Nunan JG, Wiliamson WB, Robota HJ, Henk MG (1995) SAE Tech Pap No. 950258
16. Nieuwenhuys BE (1999) Adv Catal 44:259–328
17. Heemeier M, Frank M, Libuda J, Wolter K, Kuhlenbeck H, Baumer M, Freund HJ (2000) Catal Lett 68:19–24
18. Stoyanovskii VO, Vedyagin AA, Aleshina GI, Volodin AM, Noskov AS (2009) Appl Catal B Environ 90:141–146
19. Vedyagin AA, Gavrilov MS, Volodin AM, Stoyanovskii VO, Slavinskaya EM, Mishakov IV, Shubin YV (2013) Top Catal 56:1008–1014
20. Vedyagin AA, Volodin AM, Stoyanovskii VO, Mishakov IV, Medvedev DA, Noskov AS (2011) Appl Catal B Environ 103:397–403
21. Vedyagin AA, Volodin AM, Stoyanovskii VO, Kenzhin RM, Slavinskaya EM, Mishakov IV, Plyusnin PE, Shubin YV (2014) Catal Today 238:80–86
22. Araya P, Díaz V (1997) J Chem Soc, Faraday Trans 93:3887–3891
23. Shubin YuV, Plyusnin PE, Korenev SV (2015) J Alloy Compd 622:1055–1060
24. Matsouka V, Konsolakis M, Yentekakis IV, Papavasiliou A, Tsetsekou A, Boukos N (2011) Top Catal 54:1124–1134
25. Zheng Q, Farrauto R, Deeba M (2015) Catalysts 5:1797–1814
26. Nazarpoor Z, Golden SJ (2014) Thermally stable compositions of OSM free of rare earth metals. U.S. Patent 8,853,121
27. Wu X, Xu L, Weng D (2004) Appl Surf Sci 221:375–383
28. Shackelford JF, Doremus RH (2008) Ceramic and glass materials: structure, properties and processing. Springer Science + Business Media, New York
29. Powder Diffraction File. PDF-2/Release 2009: International Centre for Diffraction Data. USA
30. Zotov RA, Molchanov VV, Volodin AM, Bedilo AF (2011) J Catal 278:71–77
31. Boehm HP, Knözinger H, Anderson JR, Boudart M (1983) Catalysis-science and technology, vol IV. Springer-Verlag, Berlin
32. Loong CK, Richardson JW Jr, Ozawa M (1997) J Alloy Compd 250:356–359
33. Tijburg IM, De Bruin H, Elberse PA, Geus JW (1991) J Mater Sci 26:5945–5949
34. Bowen P, Carry C (2002) Powder Technol 128:248–255
35. Medvedev DA, Rybinskaya AA, Kenzhin RM, Volodin AM, Bedilo AF (2012) Phys Chem Chem Phys 14:2587–2598
36. Gaspar AB, Dieguez LC (2000) Appl Catal A-Gen 201:241–251
37. Tessier D, Rakai A, Bozon-Verduraz F (1992) Phys Chem Chem Phys 88:741–749
38. Ciuparu D, Bensalem A, Pfefferle L (2000) Appl Catal B-Environ 26:241–255
39. Nilsson PO, Shivaraman MS (1979) J Phys C Solid State 12:1423–1427
40. Espinosa-Alonso L, de Jong KP, Weckhuysen BM (2010) Phys Chem Chem Phys 12:97–107
41. Elding LI (1972) Inorg Chim Acta 6:647–651
42. Rakai A, Tessier D, Bozon-Verduraz F (1992) New J Chem 16:869–875